










Myelin and axon pathology in multiple sclerosis assessed by myelin water and multi-shell diffusion imaging

Reza Rahmanzadeh,^{1,2} Po-Jui Lu,^{1,2}  Muhamed Barakovic,^{1,2}  Matthias Weigel,^{1,2,3} Pietro Maggi,^{4,5} Thanh D. Nguyen,⁶  Simona Schiavi,⁷ Alessandro Daducci,⁷  Francesco La Rosa,^{8,9} Sabine Schaedelin,¹ Martina Absinta,^{10,11}  Daniel S. Reich,¹⁰ Pascal Sati,^{10,12} Yi Wang,⁶ Meritxell Bach Guadra,^{8,9} Ernst-Wilhelm Radue,¹  Jens Kuhle,² Ludwig Kappos² and  Cristina Granziera^{1,2}

Damage to the myelin sheath and the neuroaxonal unit is a cardinal feature of multiple sclerosis; however, a detailed characterization of the interaction between myelin and axon damage *in vivo* remains challenging.

We applied myelin water and multi-shell diffusion imaging to quantify the relative damage to myelin and axons (i) among different lesion types; (ii) in normal-appearing tissue; and (iii) across multiple sclerosis clinical subtypes and healthy controls. We also assessed the relation of focal myelin/axon damage with disability and serum neurofilament light chain as a global biological measure of neuroaxonal damage. Ninety-one multiple sclerosis patients (62 relapsing-remitting, 29 progressive) and 72 healthy controls were enrolled in the study.

Differences in myelin water fraction and neurite density index were substantial when lesions were compared to healthy control subjects and normal-appearing multiple sclerosis tissue: both white matter and cortical lesions exhibited a decreased myelin water fraction and neurite density index compared with healthy ($P < 0.0001$) and peri-plaque white matter ($P < 0.0001$). Periventricular lesions showed decreased myelin water fraction and neurite density index compared with lesions in the juxtacortical region ($P < 0.0001$ and $P < 0.05$). Similarly, lesions with paramagnetic rims showed decreased myelin water fraction and neurite density index relative to lesions without a rim ($P < 0.0001$). Also, in 75% of white matter lesions, the reduction in neurite density index was higher than the reduction in the myelin water fraction. Besides, normal-appearing white and grey matter revealed diffuse reduction of myelin water fraction and neurite density index in multiple sclerosis compared to healthy controls ($P < 0.01$). Further, a more extensive reduction in myelin water fraction and neurite density index in normal-appearing cortex was observed in progressive versus relapsing-remitting participants. Neurite density index in white matter lesions correlated with disability in patients with clinical deficits ($P < 0.01$, $\beta = -10.00$); and neurite density index and myelin water fraction in white matter lesions were associated to serum neurofilament light chain in the entire patient cohort ($P < 0.01$, $\beta = -3.60$ and $P < 0.01$, $\beta = 0.13$, respectively).

These findings suggest that (i) myelin and axon pathology in multiple sclerosis is extensive in both lesions and normal-appearing tissue; (ii) particular types of lesions exhibit more damage to myelin and axons than others; (iii) progressive patients differ from relapsing-remitting patients because of more extensive axon/myelin damage in the cortex; and (iv) myelin and axon pathology in lesions is related to disability in patients with clinical deficits and global measures of neuroaxonal damage.

1 Department of Medicine and Biomedical Engineering, Translational Imaging in Neurology Basel, University Hospital Basel and University of Basel, Basel, Switzerland

Received July 26, 2020. Revised December 29, 2020. Accepted January 03, 2021. Advance access publication March 9, 2021

© The Author(s) (2021). Published by Oxford University Press on behalf of the Guarantors of Brain. This is an Open Access article distributed under the terms of the Creative Commons Attribution Non-Commercial License (<http://creativecommons.org/licenses/by-nc/4.0/>), which permits non-commercial re-use, distribution, and reproduction in any medium, provided the original work is properly cited. For commercial re-use, please contact journals.permissions@oup.com

- 2 Departments of Medicine, Clinical Research and Biomedical Engineering Neurologic Clinic and Policlinic, Switzerland, University Hospital Basel and University of Basel, Basel, Switzerland
- 3 Division of Radiological Physics, Department of Radiology, University Hospital Basel, Basel, Switzerland
- 4 Department of Neurology, Lausanne University Hospital, Lausanne, Switzerland
- 5 Cliniques universitaires Saint Luc, Université catholique de Louvain, Brussel, Belgium
- 6 Department of Radiology, Weill Cornell Medical College, New York, NY, USA
- 7 Department of Computer Science, University of Verona, Verona, Italy
- 8 Signal Processing Laboratory (LTSS), Ecole Polytechnique Fédérale de Lausanne (EPFL), Lausanne, Switzerland
- 9 Radiology Department, Center for Biomedical Imaging (CIBM), Lausanne University and University Hospital, Lausanne, Switzerland
- 10 Translational Neuroradiology Section, National Institute of Neurological Disorders and Stroke, NIH, Bethesda, MD, USA
- 11 Department of Neurology, Johns Hopkins School of Medicine, Baltimore, MD, USA
- 12 Department of Neurology, Cedars-Sinai Medical Center, Los Angeles, CA, USA

Correspondence to: Professor Cristina Granziera
 Department of Biomedical Engineering
 Translational Imaging in Neurology (ThINk) Basel
 University of Basel Gewerbestrasse 14, 4123 Allschwil, Switzerland
 E-mail: cristina.granziera@usb.ch

Keywords: multiple sclerosis; myelin water imaging; diffusion microstructural modelling; neurodegeneration; demyelination

Abbreviations: EDSS = Expanded Disability Status Scale; MCMDI = multi-compartment microscopic diffusion imaging; MWF = myelin water fraction; NAGM = normal-appearing grey matter; NAWM = normal-appearing white matter; NDI = neurite density index; NODDI = neurite orientation dispersion and density imaging; PMS = progressive multiple sclerosis; RRMS = relapsing remitting multiple sclerosis

Introduction

The presence of myelin and axon damage—and the interaction between them—are major pathological drivers of neurological disability in multiple sclerosis.¹ Still, up to the present time, the investigation of myelin and axon properties in multiple sclerosis patients *in vivo* has been challenging, owing to the heterogeneity of the disease but also to the lack of appropriate methodologies to study the complex interplay between the pathological changes occurring to the myelin sheet and the neuroaxonal unit.

Multiple sclerosis lesions are heterogeneous in terms of cellular composition of the inflammatory infiltrate, target of injury and degree of demyelination and axonal loss.² In neuropathological studies, lesion-wise variation has been observed intra- and inter-individually and among lesions in different locations and at different stages of development.^{3,4} In fact, periventricular lesions exhibit much more pronounced myelin and axon loss than juxtacortical lesions.^{5,6} On the other hand, chronic active lesions show a more pronounced axon loss in their inactive centre compared to other lesions (e.g. acute and inactive), and a surrounding rim with myelin-phagocytosing macrophages and axon end-bulbs.⁷ Also, previous pathological and imaging studies revealed that axon/myelin damage is not limited to the plaque area, but rather extends to the tissue surrounding it.^{8,9}

The pathological characteristics of white matter lesions seem to be similar between plaques found in patients with relapsing remitting multiple sclerosis (RRMS) and progressive multiple sclerosis (PMS).² Nevertheless, the low efficacy of immunomodulatory therapeutics and higher disability in PMS patients suggest that there is more extensive diffuse pathology in PMS compared to RRMS. This damage encompasses pronounced myelin loss, axon transection/degeneration, and clusters of activated

microglia in normal-appearing white and grey matter (NAWM, NAGM).^{10,11}

MRI has provided a precious window into the neuropathological features of multiple sclerosis in living patients. Magnetization transfer imaging (MTI) and diffusion tensor imaging (DTI) showed the presence and extent of focal and diffuse changes in both RRMS and PMS patients by exploiting measures such as magnetization transfer ratio, median diffusivity and fractional anisotropy.¹² Yet, despite the applied measures demonstrating good sensitivity to pathological changes in multiple sclerosis patients, they lack specificity for both myelin and axon damage.

Myelin water imaging (MWI)¹³ and biophysical models of diffusion MRI¹⁴ provide more specific surrogate measures of myelin and axon integrity than DTI and MTI. MWI quantifies the water between myelin layers by distinguishing multiple water components in T₂ relaxometry data and supports with measures (e.g. myelin water fraction, MWF), which have been validated post-mortem.^{15,16} Neurite orientation dispersion and density imaging (NODDI) mathematically models multi-shell diffusion data to estimate axon and dendrite density (neurite density index, NDI) and the orientation of tissue components in the CNS.¹⁷ The advantage of NODDI over DTI is that NODDI does not assume a Gaussian distribution of diffusion processes and, hence, models non-Gaussian diffusion in biological tissue providing more specific measures of tissue microstructure.^{18,19} Multi-compartment microscopic diffusion imaging (MCMDI) is an alternative technique to the NODDI model that provides estimates of intra- and extra-neurite compartments in the brain, which has also been applied to multiple sclerosis patients.^{20,21}

Thanks to MRI hardware and software developments, it is now possible to acquire MWI and multi-shell diffusion data in clinically compatible protocols, which allow us to simultaneously assess the

presence, extent and interplay between myelin and axon damage in living multiple sclerosis patients. Besides, MWI and multi-shell diffusion may be combined with other pulse sequences—such as inversion-contrast magnetization-prepared 2 rapid gradient echo sequence (MP2RAGE)²² and 3D segmented echo planar imaging (3D-EPI)²³—that permit us to identify specific lesion subtypes such as cortical lesions and chronic active lesions.

The goal of the current work was to exploit MWI and multi-shell diffusion imaging to investigate the relative distribution of myelin and axonal damage (i) in distinct lesion types—as identified with the help of MP2RAGE and 3D EPI; (ii) in NAWM and NAGM; and (iii) across different disease phenotypes, as compared to healthy control subjects. Further, we then assessed the relationship between NDI/MWF measures and neurofilament light chain, to determine whether those measures are related to global biological measures of neuroaxonal damage in living patients.

Materials and methods

Participants

We enrolled 91 multiple sclerosis patients (62 RRMS and 29 PMS) and 72 healthy controls (Table 1). The inclusion criteria were: (i) multiple sclerosis diagnosis according to McDonald criteria 2018²⁴ and diagnosis of active RRMS or inactive PMS as defined by Lublin et al.²⁵; (ii) absence of any concomitant psychiatric or neurological disease (excluding headache); and (iii) absence of contra-indication to MRI. The ethical review committee of the University Hospital Basel (IRB of Northwest Switzerland) approved the study, and all participants entered the study following written consent.

Clinical assessment

Multiple sclerosis disability was assessed using Neurostatus-EDSS (www.neurostatus.net)²⁶ by certified neurologists at Basel University Hospital. There were only nine patients with Expanded Disability Status Scale (EDSS) 0 and eight with EDSS 1 in our cohort: those patients showed various levels of mean MWF and NDI in lesions despite the absence of measurable clinical disability. Because this absence of a clinical correlate of focal damage in those patients might be due to several factors encompassing functional reserve and compensatory mechanisms, we decided to focus on patients with clinical disability, where the relationship

Table 1 Patient and control demographics

	Multiple sclerosis subjects	Healthy control subjects
Sex, n (male/female)	91 (35/56)	72 (29/43)
Age, years, mean ± SD	46 ± 14	36 ± 12
EDSS score, median (range)	2.5 (0–8)	–
Disease course, RR/PMS	62/29	–
Disease-modifying therapy (n)	Untreated (10) Interferon-beta (1) Glatiramer acetate (1) Dimethyl fumarate (13) Fingolimod (5) Natalizumab (2) Rituximab (10) Ocrelizumab (49)	–

SD = standard deviation.

between focal damage and clinical deficits might be less confounded.

Magnetic resonance acquisition and metrics computation

MRI was performed on a 3 T whole-body magnetic resonance system (Magnetom Prisma, Siemens Healthcare) using a 64-channel phased-array head and neck coil for radio frequency reception. The MRI protocols included: (i) 3D FLAIR (repetition time/echo time/inversion time = 5000/386/1800 ms) and MP2RAGE (repetition time/inversion time 1/inversion time 2 = 5000/700/2500 ms) both with 1 mm³ isotropic spatial resolution; (ii) fast acquisition with spiral trajectory and adiabatic T2prep (FAST-T2) [spiral repetition time/echo time = 7.5/0.5 ms, six T2prep times = 0 (T2prep turned off), 7.5, 17.5, 67.5, 147.5, 307.5 ms, voxel size = 1.25 × 1.25 × 5 mm³, scan time = 4.5 min, as described in Nguyen et al.²⁷]; (iii) multi-shell diffusion (repetition time/echo time/δ/Δ/resolution = 4.5 s/75 ms/19 ms/36 ms/1.8 mm³ isotropic with b-values 0/700/1000/2000/3000 s/mm² with 12/6/20/45/66 measurements, respectively, per shell and a diffusion acquisition with 12 measurements of b-value 0 s/mm² with reversed phase encoding; as well as (iv) 3D segmented EPI with submillimetre isotropic resolution (repetition time/echo time/resolution = 64 ms/35 ms/0.67 × 0.67 × 0.67 mm³), providing both T₂* magnitude and phase contrast.

In FAST-T2, the robustness of the MWF map against noise propagation is achieved by judiciously sampling the T₂ signal at a very short echo time (0.5 ms) to maximize sensitivity to the fast-decaying myelin water component, and also by utilizing a local spatial smoothing constraint in the multi-exponential data fitting (Fig. 1).²⁷ As in Nguyen et al.,²⁷ we used an adiabatic T2prep design based on a 0° modified BIR-4 pulse.²⁸ This symmetric pulse consisted of a reverse half passage, a full passage, and a half passage adiabatic pulse separated by two equal time delays of length echo time/2. A previously proposed spatially local smoothness constraint²⁹ was incorporated in the three-pool non-linear fitting by jointly solving the minimization problem over all brain voxels at once. The regularization parameter λ was determined by calculating MWF maps for different λ values in a healthy subject and selecting the one that provided an MWF map with the best visual quality. This optimized value was then fixed for all of the subjects enrolled in this study.

Diffusion images were denoised³⁰ and corrected for motion and eddy-currents.³¹ Two different diffusion models were used. NODDI,¹⁷ which is a state-of-the-art model aiming at characterizing the neurite orientation dispersion (Fig. 1), but has two strong assumptions: (i) fixed diffusivity for all the voxels in the brain tissue whole-brain voxels; and (ii) applicability to single-bundle voxels (very few locations in the brain). Due to these limitations we investigated a second advanced diffusion model, MCDMI.²¹ MCDMI integrates the spherical mean technique to handle orientation dispersion and fibre crossing populations, allowing more accurate estimations in whole-brain voxels. From both models, we estimated the NDI, which corresponds putatively to the intra-axonal volume fraction. The results are termed NODDI-NDI and MCDMI-NDI.

Phase images collected with a 0.67 mm isotropic 3D-EPI acquisition²³ were recently shown to provide high sensitivity at 3 T for detecting chronic active lesions with paramagnetic rims.³² These phase images are interpreted after an automatic analytical phase unwrapping procedure and removal of large background gradients with Gaussian filtering (Fig. 1).

Quantitative susceptibility mapping (QSM) is a field-to-source inversion method to map the local susceptibility sources in the tissue from the shift in the magnetic field created by these

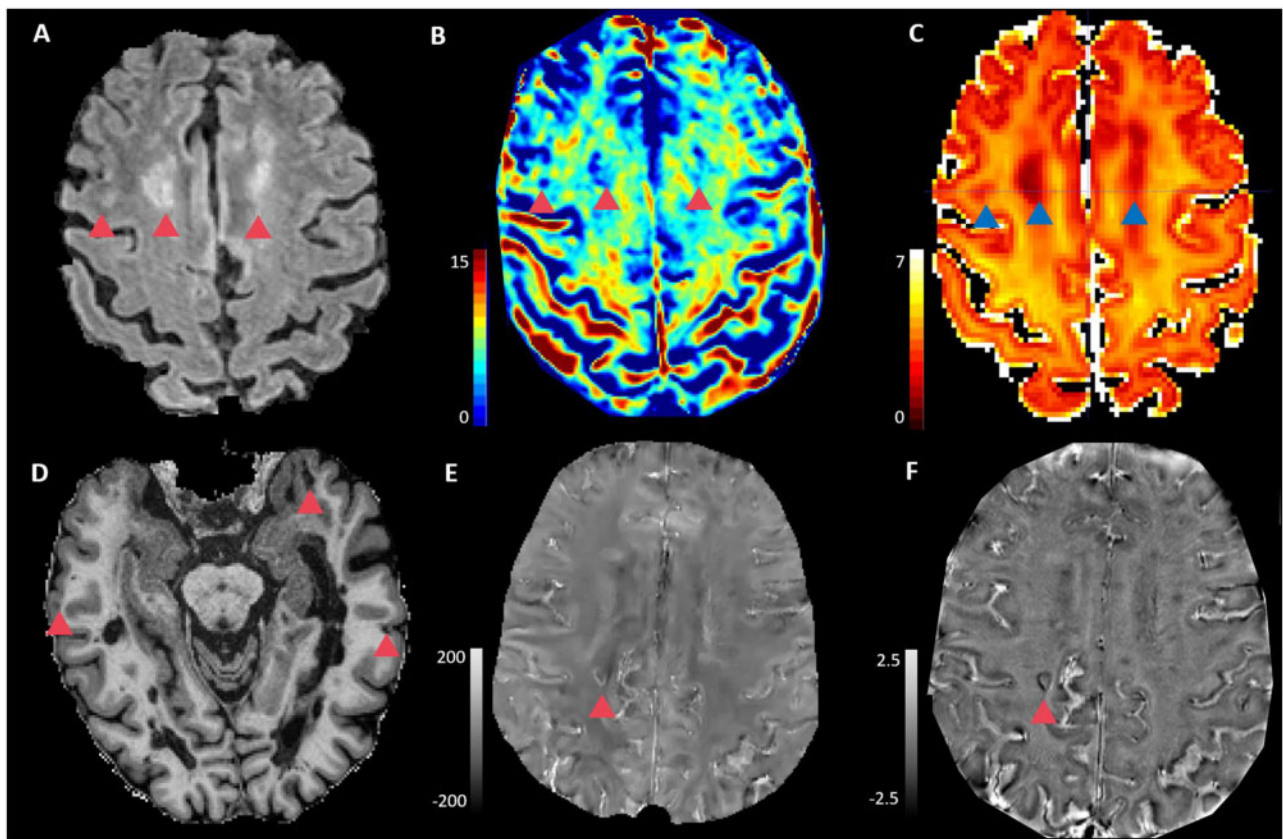


Figure 1 Axial images in one exemplary multiple sclerosis patient. (A) FLAIR, (B) MWF map, (C) NODDI-NDI map, (D) MP2RAGE, (E) 3D-EPI QSM and (F) 3D-EPI unwrapped phase. Red/Blue triangles show white matter lesions (A–C), cortical lesions (D) and lesions with paramagnetic rim (E and F).

sources which can be measured from gradient echo data. In this study, QSM were reconstructed from 3D EPI data by unwrapping phase, removing the background field through Projection onto Dipole Fields algorithm, and using the morphology-enabled dipole inversion algorithm to compute the susceptibility from the local field as in Liu *et al.*³³ (Fig. 1).

Lesion identification and segmentation

Automatic segmentation of white matter lesions was performed by using an in-house deep-learning based method.³⁴ This approach consists of a cascade of two convolutional neural networks and was adapted to take as input FLAIR and MP2RAGE MRI contrasts. Manual correction of automatic white matter lesion masks was performed on FLAIR (by R.R. and C.G.). Manual detection of cortical lesions on MP2RAGE was done by two experienced readers by consensus (R.R. and C.G.), and cortical lesions were divided into intra-cortical lesions and leukocortical lesions according to Guerts *et al.*³⁵

Lesions with a paramagnetic rim (Rim+) on both 3D-EPI unwrapped phase and 3D-EPI QSM images were identified by two raters (P.M. and M.A. for phase and R.R. and C.G. for QSM) and were then manually refined by separating confluent Rim+ and Rim-lesions in original white matter lesion masks on FLAIR. Of 265 lesions on unwrapped phase and 183 lesions on EPI QSM were Rim+, 159 lesions exhibited paramagnetic rims on both sequences.

To estimate the relative proportion of myelin and axonal damage in white matter lesions, we calculated the %MWF and %NDI reduction in white matter lesions as follows: (mean MWF/NDI in the

mirror region of interest in the contralateral hemisphere – mean MWF/NDI in lesion) $\times 100$ / the value in the mirror region of interest in contralateral hemisphere. For this purpose, all lesions exhibiting contralateral normal-appearing mirror areas were selected in the lesion masks. In total, 85 lesions were selected and the mirror regions of interest were then manually contoured.

White matter and cortex segmentation

To segment the brain into whole white matter, cortex, deep grey matter structures, and ventricles we used the imaging software package FreeSurfer (v.6.0, surfer.nmr.mgh.harvard.edu).³⁶ NAWM and NAGM masks were obtained by subtracting white matter and cortical lesion masks from white matter and cortical masks. An in-house algorithm was used to automatically produce two two-voxel layers of NAWM surrounding the lesions; hereafter denoted as peri-plaque-1st (PP-1st) and peri-plaque-2nd (PP-2nd). White matter masks were divided into three regions: periventricular (i.e. area within 3 mm from ventricle wall), juxtacortical (i.e. area in 3 mm from the boundary between white matter and cortex), and deep white matter (i.e. area between periventricular and juxtacortical).

Voxel-based analyses for normal-appearing white matter

NAWM maps were co-registered patient-wise to a reference brain (standard MNI152 space) using a rigid-body registration in FMRIB Software Library (FSL).³⁷ As previously performed,³⁸ in NAWM we excluded voxels that were (i) not present in at least 50% of subjects; and (ii) filled missing data with the group mean value of those

voxels present in group subjects. We then performed a voxel-wise comparison of MWF, NODDI-NDI, MCMDI-NDI maps between patients and control subjects by using the randomize tool of FSL with threshold-free cluster enhancement (TFCE) clustering. *P*-values < 0.01 were considered statistically significant.

Vertex-wise analysis for normal-appearing grey matter

A customized volume-to-surface mapping algorithm was applied to voxels assigned to the grey matter ribbon by Free Surfer—i.e. voxels with voxel centres located between the white and pial surfaces were registered and scattered into a standard surface. A smoothing kernel of 10-mm full-width at half-maximum was used. The whole-depth NAGM of MWF, NODDI-NDI, and MCMDI-NDI maps was resampled on inflated cortex, and a generalized linear model (GLM) analysis was conducted for comparison among groups with age and sex as covariates. *P*-values < 0.01 were considered statistically significant.

Serum neurofilaments quantification

Neurofilaments were quantified in serum collected within 1 month of the MRI (serum neurofilaments) using a single molecule array assay.³⁹

Statistical analysis

Based on previous histopathology and imaging findings, we hypothesized that: (i) cortical/white matter lesions and NAWM and NAGM are damaged compared to healthy tissue in healthy controls and show different extents of myelin and axonal damage; (ii) chronic active lesions exhibit more axonal and myelin damage compared to other white matter lesions; (iii) peri-plaque tissue is abnormal, and the extent of pathology is proportional to lesion pathology and decreases with distance from lesions; (iv) myelin damage outweighs axon damage in multiple sclerosis lesions; (v) the extent of damage differs between RRMS and PMS patients; and (vi) clinical disability and serum neurofilament levels are associated with myelin and axonal damage.

Statistical analysis was performed using R-project (www.r-project.org) and GraphPad Prism version 8.0.0 for Windows, GraphPad Software, San Diego, California USA. Kolmogorov-Smirnov's test was used to assess the normality of data. Paired *t*-test, non-parametric Mann-Whitney test, and Kruskal-Wallis test with Dunn's test for multiple comparisons correction, were used for paired two-group analysis, unpaired two-group analysis, and more-than-three group analysis, respectively. All values, including intra-lesional, homogeneous non-lesional normal-appearing tissue and peri-plaque tissues, were automatically extracted in both lesion-wise and average patient-wise manners.

For serum neurofilament measures, a logarithmic transformation was applied to comply with normality assumption. Correlation studies between MRI measures, serum neurofilaments and EDSS were performed using a GLM, with age and gender as covariates. The GLM was performed for the whole sample and for patients with clinical deficits only (EDSS > 1). A two-tailed *P* < 0.05 was considered statistically significant.

To model the respective contribution of NDI and MWF to the separation of white matter lesion/cortical lesion versus the corresponding normal-appearing tissue and the relative normal tissue in healthy controls, we used multinomial logistic regression and a penalized⁴⁰ logistic regression as sensitivity analysis.

Data availability

The data that support the findings of this study are available upon reasonable request.

Results

Cortical and white matter lesions

The number, volume, and regional distribution of white matter lesions and cortical lesions are detailed in Table 2. White matter lesions were found in all multiple sclerosis patients: periventricular lesions in 89/91 (98%) patients, juxtacortical lesions in 91/91 (100%) patients. Cortical lesions were found in 41/91 (45%) multiple sclerosis patients, leukocortical lesions in 38/91 (42%), and intracortical lesions in 16/91 (18%). Cortical lesions were more common in PMS than in RRMS (*P* = 0.017). The quantity of lesions with paramagnetic rims detectable in both EPI phase and EPI QSM images was not different in PMS when compared to RRMS (all *P* > 0.05).

Axon and myelin in distinct multiple sclerosis lesion types

In white matter lesions, the average MWF and NODDI-NDI were lower compared to NAWM in patients and white matter of healthy control subjects (all *P* < 0.0001, Fig. 2A and B). The average MCMDI-NDI was also lower compared to NAWM and white matter of healthy controls (both *P* < 0.0001, Supplementary Fig. 1). In cortical lesions, the average NODDI-NDI and MWF were lower compared to NAGM in patients and grey matter of healthy controls (both *P* < 0.0001, Fig. 1D and E). Also, the average MCMDI-NDI was lower compared to NAGM and grey matter of healthy controls (*P* = 0.014 and *P* = 0.018, respectively) (Supplementary Fig. 1).

Figure 1C shows that myelin and axon content in white matter lesions were proportional to each other (Spearman's *r* = 0.4901, *P* < 0.0001) and there was a large variation in MWF and NODDI-NDI in white matter lesions. Periventricular lesions exhibited lower MWF and NODDI-NDI compared to juxtacortical lesions (Fig. 2G–I, *P* < 0.0001 and *P* = 0.024, respectively). MCMDI-NDI was also lower in periventricular lesions compared to juxtacortical lesions (*P* < 0.0001, Supplementary Fig. 1). Although there was no difference in MWF between periventricular and juxtacortical regions in healthy controls (*P* = 0.0741), NODDI-NDI and MCMDI-NDI were lower in periventricular regions compared to juxtacortical regions in healthy controls (both *P* < 0.0001). Like white matter lesions, cortical lesions exhibited proportional myelin and axon

Table 2 Lesion count and volume in white matter and cortical lesions

Lesion location	Median (range)	Mean ± SD
Cortical lesion count	0 (0–113)	6.5 ± 17
Cortical lesion volume, mm ³	0 (0–1783)	195 ± 439
IC lesion count	0 (0–25)	0.6 ± 2.7
IC lesion volume, mm ³	0 (0–236)	8.1 ± 30
LC lesion count	0 (0–88)	4.9 ± 13
LC lesion volume, mm ³	0 (0–1718)	178 ± 406
White matter lesion count	47 (1–201)	54 ± 42
White matter lesion volume, mm ³	5115 (23–64 359)	8602 ± 10 881
PV lesion count	8 (0–27)	10 ± 7
PV lesion volume, mm ³	285 (0–6650)	913 ± 1381
JC lesion count	31 (1–152)	40 ± 34
JC lesion volume mm ³	1847 (7–36 435)	3885 ± 5623

IC = intracortical; JC = juxta-cortical; LC = leuko-cortical; PV = periventricular; SD = standard deviation.

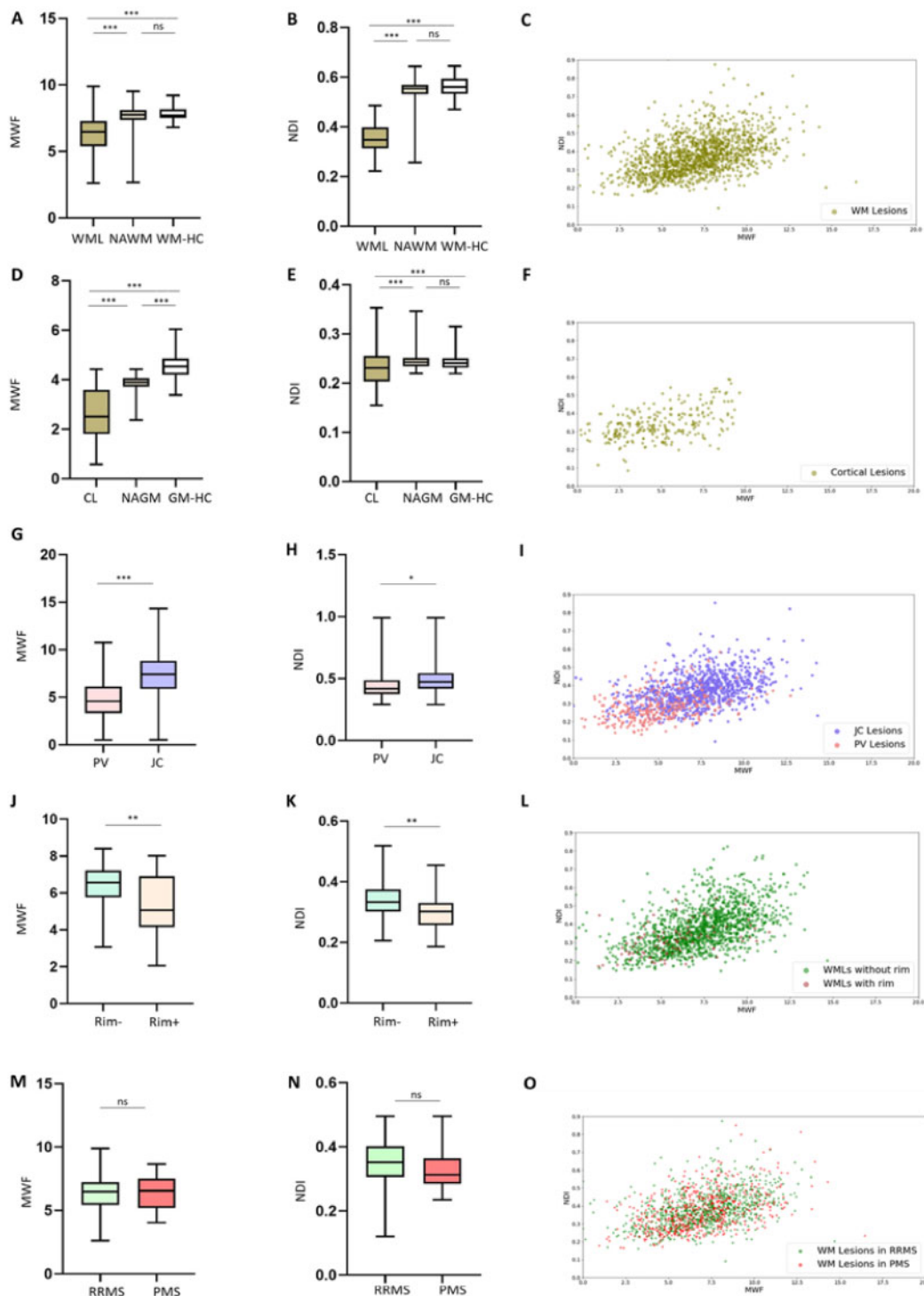


Figure 2 MWF and NODDI-NDI in different types of multiple sclerosis lesions. (A and B) Box plots showing that MWF and NDI in white matter lesions (WMLs) is lower than MWF and NDI in NAWM and white matter in healthy controls (WM-HC). (C) NDI-MWF scatter plots in white matter lesions. (D and E) Box plots showing that MWF and NDI in cortical lesions (CL) is lower than in NAGM and grey matter in healthy controls (GM-HC). (F) NDI-MWF scatter plots in cortical lesions. (G and H) MWF and NDI are lower in periventricular (PV) lesions than in juxtacortical (JC) lesions. (I) NDI-MWF scatter plot in periventricular and juxtacortical lesions. (J and K) MWF and NDI are lower in Rim+ lesions than in Rim- lesions. (L) NDI-MWF scatter plot for white matter lesions with and without paramagnetic phase rim on both 3D EPI unwrapped phase and 3D EPI QSM images. (M and N) MWF and NDI were not different between RRMS and PMS. (O) NDI-MWF scatter plots for white matter lesions in RRMS versus PMS. NDI; NODDI-NDI. *** $P < 0.0001$; ** $P < 0.001$; * $P < 0.05$. ns = not significant; WM = white matter.

content (Spearman’s $r = 0.4372$, $P < 0.0001$, Fig. 2F), yet there was large variation in MWF and NODDI-NDI across cortical lesions. Rim+ lesions exhibited lower NODDI-NDI and MWF compared to

Rim- lesions (both $P < 0.001$, Fig. 2J–L). MCMDI-NDI was also lower in Rim+ lesions compared to Rim- lesions ($P = 0.001$, Supplementary Fig. 1).

We modelled NDI with MWF by using a multinomial logistic regression with (i) MWF and NDI as independent variables; and (ii) tissue types (i.e. lesions, normal-appearing tissue and healthy tissue) as dependent variables. By doing this for both white matter and cortical lesions, we determined that both MWF and NDI explain to a certain extent the differences between the three tissue types, but NDI appears to separate the three tissue types better than MWF (Table 3 and Supplementary Fig. 2) in white matter; for the model related to cortical lesions neither NDI nor MWF could significantly explain the separation of the tissue types. To address the separation between lesions versus healthy tissue and lesions versus normal-appearing tissue, we further estimated two penalized logistic regression models as suggested⁴⁰ as sensitivity analysis. These analyses confirm the superior role of NDI in separating tissue type for white matter lesions, show a trend for NDI also for separating cortical lesions from normal-appearing tissue and a very small but significant contribution of MWF in separating cortical lesions from healthy tissue.

Pathology around multiple sclerosis lesions

Peri-plaque tissue in white matter and cortical lesions

MWF and NODDI-NDI increased from the white matter lesions to PP-1st and from PP-1st to PP-2nd (Fig. 3A–C); MWF: all $P < 0.0001$, NODDI-NDI: all $P < 0.0001$. In addition, MCMDDI-NDI increased from white matter lesions to PP-1st and from PP-1st to PP-2nd (all $P < 0.0001$, Supplementary Fig. 1). However, MWF, NODDI-NDI, and MCMDDI-NDI

were not significantly different among white matter-HC (healthy controls), PP-1st, and PP-2nd (all $P > 0.05$).

Cortical lesions had lower MWF compared to PP-1st and PP-2nd (both $P < 0.001$). Cortical lesions also had lower NODDI-NDI compared to PP-1st and PP-2nd ($P = 0.03$ and $P < 0.001$, respectively). However, the average NODDI-NDI and MWF in PP-1st and PP-2nd were similar (Fig. 3D and E). MCDMI-NDI is significantly lower in cortical lesions compared to PP-1st and PP-2nd (both $P < 0.05$, Supplementary Fig. 1). However, MWF, NODDI-NDI and MCMDDI-NDI were not different among grey matter-HC, PP-1st, and PP-2nd (all $P > 0.05$).

Peri-plaque tissue in lesions with and without a paramagnetic rim

NODDI-NDI, MCMDDI-NDI and MWF were not different in PP-1st and PP-2nd around the Rim+ lesions compared to Rim- lesions (all $P > 0.05$).

Normal-appearing brain tissue

Normal-appearing white matter

The average MWF and NODDI-NDI values in NAWM was not significantly different from that in white matter of healthy controls (Fig. 2). However, voxel-wise analysis using TFCE randomized clustering showed that (i) both MWF and NODDI-NDI were diffusely reduced in some clusters of NAWM voxels compared to white

Table 3 Multinomial and penalized (Firth's) logistic regression for white matter and cortical brain regions

Comparison	Variable	OR	CI	P-value
White matter regions				
Multinomial logistic regression				
WMLs versus NAWM	Intercept	12 030 141.99		
WMLs versus NAWM	NDI	0.00	[0.00–0.00]	<0.01
WMLs versus NAWM	MWF	2.46	[1.14–5.29]	0.0214
WMLs versus WM-HC	Intercept	27 040 504 475 680.04		
WMLs versus WM-HC	NDI	0.00	[0.00–0.00]	<0.01
WMLs versus WM-HC	MWF	2.59	[1.03–6.52]	0.0425
Penalized logistic regression: WMLs versus WM-HC				
WMLs versus WM-HC	Intercept	250 871 232 425 437 373 029 656 035 328.00		
WMLs versus WM-HC	NDI	0.00	[0.00–0.00]	<0.01
WMLs versus WM-HC	MWF	0.47	[0.13–2.97]	0.343
Penalized logistic regression: WMLs versus NAWM				
WMLs versus NAWM	Intercept	3 106 304.83		
WMLs versus NAWM	NDI	0.00	[0.00–0.00]	<0.01
WMLs versus NAWM	MWF	2.22	[1.11–4.76]	0.0234
Cortical regions				
Multinomial logistic regression				
CLs versus NAGM	Intercept	16.82		
CLs versus NAGM	NDI	0.00	[0.00–3.15]	0.0643
CLs versus NAGM	MWF	1.19	[0.48–2.94]	0.7104
CLs versus GM-HC	Intercept	956 307.92		
CLs versus GM-HC	NDI	0.02	[0.00–7 597 683 390.68]	0.767
CLs versus GM-HC	MWF	0.04	[0.01–0.14]	<0.01
Logistic regression: CLs versus GM-HC				
CLs versus GM-HC	Intercept	917.72		
CLs versus GM-HC	NDI	0.02	[0.00–6 283 872.23]	0.686
CLs versus GM-HC	MWF	0.21	[0.09–0.48]	<0.01
Logistic regression: CLs versus NAGM				
CLs versus NAGM	Intercept	8.88		
CLs versus NAGM	NDI	0.00	[0.00–8.57]	0.0849
CLs versus NAGM	MWF	1.11	[0.51–2.43]	0.7870

CI = confidence interval; CLs = cortical lesions; GM-HC = grey matter in healthy controls; OR = odds ratio; WM-HC = white matter in healthy controls; WML = white matter lesion.

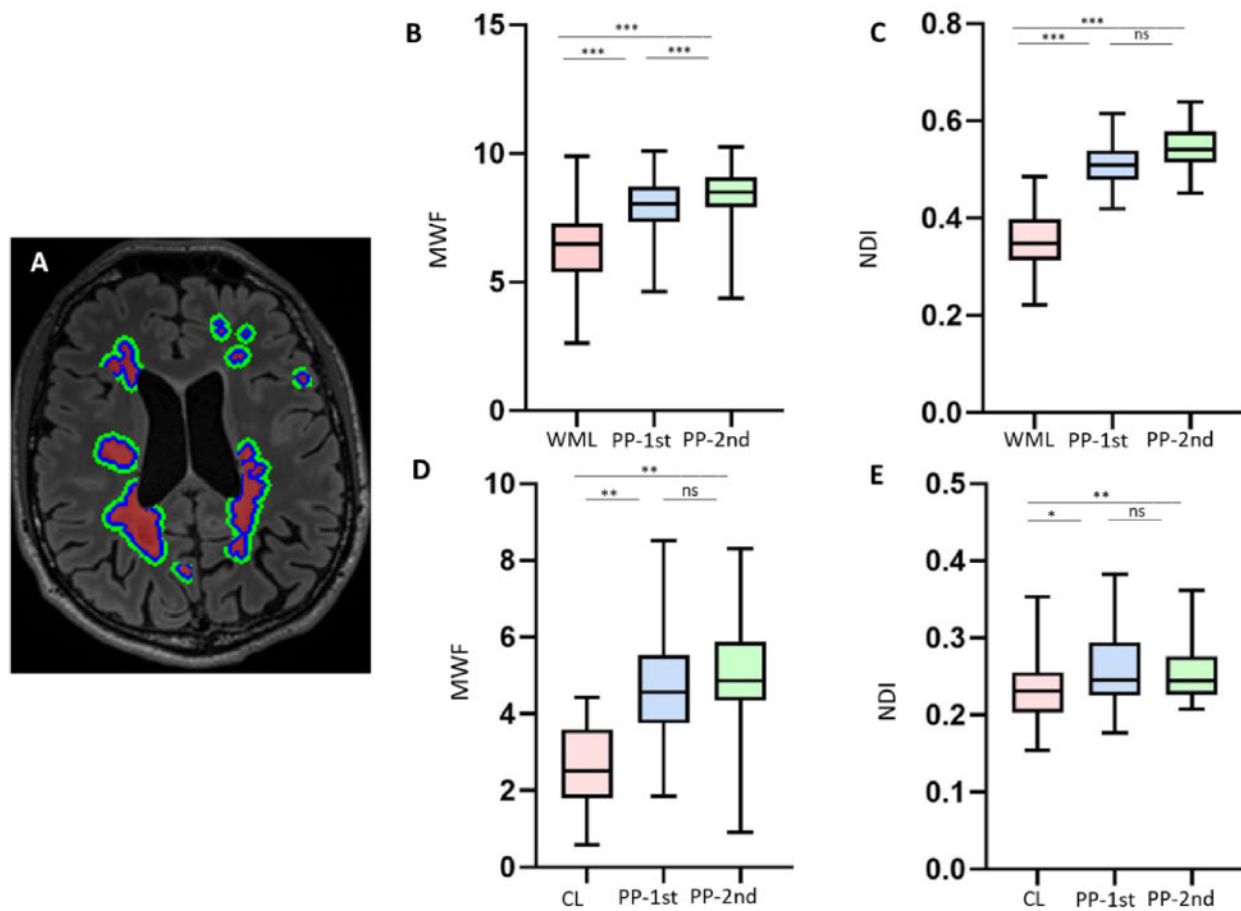


Figure 3 Peri-plaque white matter around multiple sclerosis lesions. (A) Axial 3D FLAIR image [with segmentation of white matter lesions (WMLs; red), PP-1st (blue) and PP-2nd (green)]. (B and C) Box plots showing that MWF and NDI gradually increase from white matter lesions to PP-1st and PP-2nd. (D and E) Box plots showing that MWF and NDI in cortical lesions (CL) are less than in PP-1st and PP-2nd. *** $P < 0.0001$; ** $P < 0.001$; * $P < 0.05$. ns = not significant.

matter of controls (Fig. 4, $P < 0.01$); and (ii) the area of NDI reduction exceeded the area of MWF reduction. The voxel-wise analysis performed with MCDMI-NDI maps showed similar results to that obtained with NODDI-NDI.

Normal-appearing grey matter

The average MWF value in NAGM was lower compared to grey matter of healthy controls ($P < 0.0001$). The average NODDI-NDI value in NAGM was not significantly different from grey matter of healthy controls (Fig. 1). Yet, vertex-wise cortical surface analysis of MWF and NODDI-NDI showed areas in which MWF and NODDI-NDI were reduced in multiple sclerosis NAGM compared to grey matter of healthy controls (Fig. 4, $P < 0.01$). Vertex-wise analysis performed with MCDMI-NDI maps showed similar results to that obtained with NODDI-NDI.

Axon versus myelin pathology

White matter lesions showed a variable reduction in MWF and NODDI-NDI (0.4–80% MWF; 6–72% NODDI-NDI) compared to contralateral mirror region of interest in NAWM (Fig. 5A and Supplementary Fig. 2). Percentage MWF reduction was less than %NODDI-NDI reduction in white matter lesions ($P < 0.0001$) (Fig. 5B). In 26% of lesions the %MWF reduction was more than the %NODDI-NDI reduction, and in 74% of lesions the %NODDI-NDI was more than the %MWF reduction. There was no difference in %MWF and

%NODDI-NDI among periventricular, deep white matter, and juxtacortical lesions or between RRMS and PMS (all $P > 0.05$).

Relapsing-remitting versus progressive multiple sclerosis patients

The average NODDI-NDI and MWF in white matter lesions were not different between RRMS and PMS patients (both $P > 0.05$). In accordance, lesion-wise analysis revealed a similar pattern of NDI and MWF distribution in PMS and RRMS lesions (Fig. 2M–O).

There was no difference in voxel-wise analysis in NODDI-NDI and MWF across NAWM voxels between RRMS and PMS. However, vertex-wise analysis showed areas across NAGM in which MWF and NODDI-NDI were lower in PMS compared to RRMS (Fig. 4, $P < 0.01$).

Correlation analysis between advanced MRI measures, disability and serum neurofilaments

MWF and NDI in white matter lesions did not correlate with EDSS when the entire cohort of patients was considered. However, a *post hoc* sensitivity analysis found that—in patients with clinical deficits (EDSS > 1)—NDI in white matter lesions was associated with EDSS (NDI: $P < 0.01$, $\beta = -10.00$; $n = 74$).

We also found that MWF and NDI in white matter lesions were related to serum neurofilaments (MWF: $P < 0.01$, $\beta = 0.13$; NDI: $P < 0.01$, $\beta = -3.60$) when the entire cohort of patients was

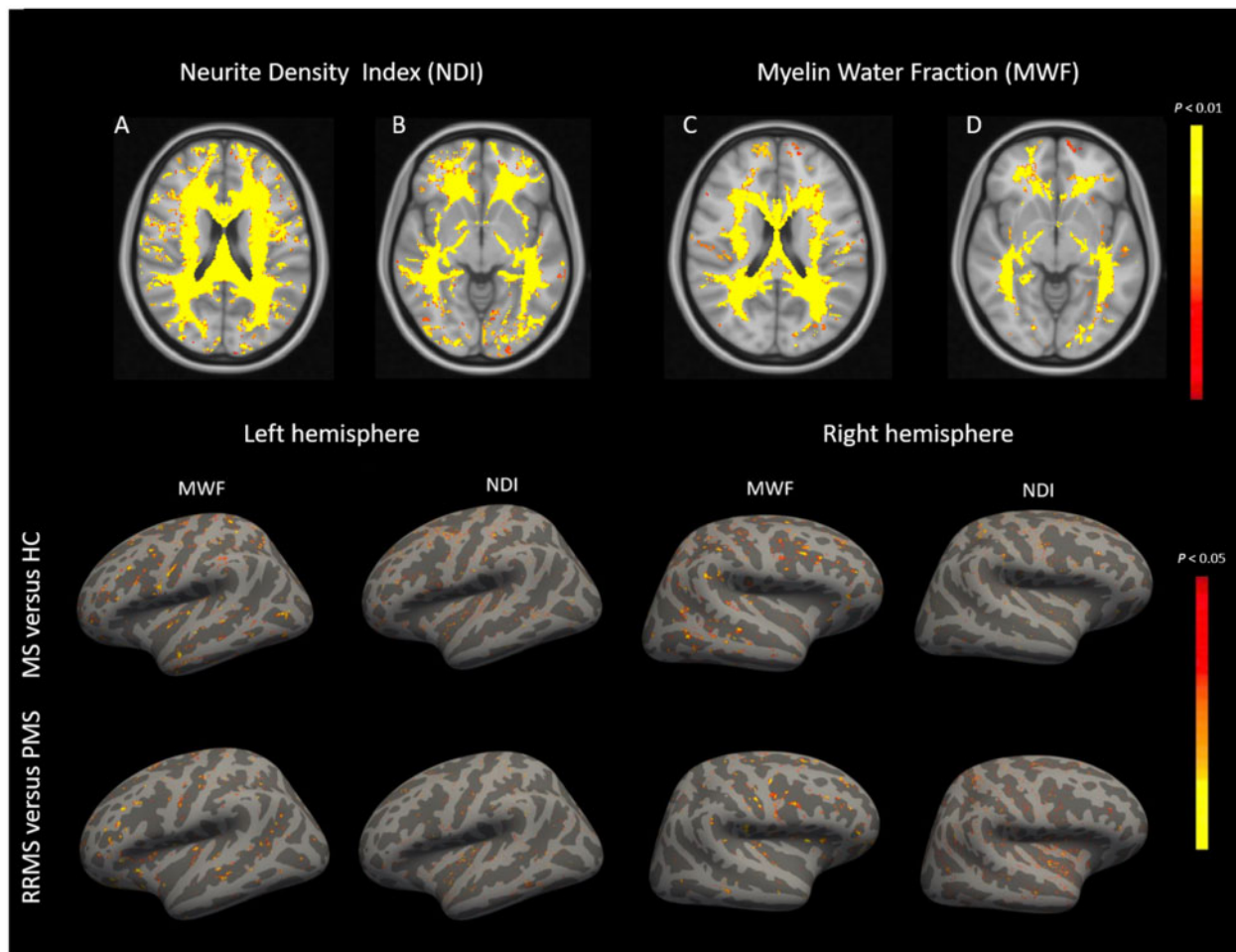


Figure 4 Comparison of NDI and MWF in normal-appearing brain tissue between patients and controls. *Top row:* (A–D) Compared to healthy subjects (HC), multiple sclerosis (MS) patients show a widespread NODDI-NDI reduction in normal-appearing white matter and—to a smaller extent—a diffuse MWF reduction. *Bottom row:* There are patchy reductions in MWF and NODDI-NDI in the normal-appearing cortical surface of multiple sclerosis patients versus healthy controls and in PMS versus RRMS patients.

considered, but this correlation was not significant after adjusting for T_2 lesion volume. However, when only patients with EDSS > 1 were considered, white matter lesion MWF correlated with serum neurofilaments ($\beta = 0.12$ and $P < 0.05$) also after covariation for T_2 lesion volume.

Discussion

In this study, we simultaneously measured MWF and NDI to explore the interplay between myelin and axonal damage in different categories of focal lesions, in normal-appearing tissue, and across multiple sclerosis subtypes compared to healthy subjects.

By leveraging MWI, multi-shell diffusion and magnetic resonance contrasts that are sensitive to both white matter lesions and cortical lesions, we studied focal axon and myelin pathology in both white matter and the cortex.

MWF and axonal density were markedly decreased in both white matter lesions and cortical lesions compared to NAWM/NAGM and healthy tissue, hereby confirming previous neuropathological studies.^{1,41} Besides, axon and myelin pathology centrifugally decreased with distance from the lesions core as shown in prior pathological and imaging works.^{10,42,43} Additionally, MWF and NDI in white matter and cortical lesions were proportional to each other—across all lesions in white matter and in the cortex—

suggesting that axon and myelin damage are synchronized and/or driven by a common pathological event.^{44,45}

However, as showed in previous neuropathology studies,¹⁹ NDI is also sensitive to myelin content. Our study provides new evidence in living subjects, that NDI contributes more than MWF to differentiate lesions from normal-appearing tissue and lesions from healthy tissue in white matter. This suggests that the reported differentiation is not driven by the myelin sensitivity of NDI, but rather by its sensitivity to the intra-axonal water compartment.

Still, neuropathological works reported that there is a substantial variability in the extent of myelin and axonal damage across multiple sclerosis lesions due to the dynamic interplay between acute and chronic inflammatory demyelination, remyelination and loss of chronically damaged axons.^{46–48}

Indeed, we have shown that periventricular lesions exhibited more myelin damage than did juxtacortical lesions, suggesting a higher rate of myelin loss and/or lower repair capacity. These findings confirm previous neuropathological and PET studies suggesting lower remyelinating capacity and higher tissue damage in periventricular compared to juxtacortical lesions.^{6,47,49} Juxtacortical regions are in fact characterized by more numerous and more efficacious oligodendrocyte precursor cells (OPCs), compared to periventricular regions^{50–52}; likewise, periventricular regions are more prone to damage due to diffusion of

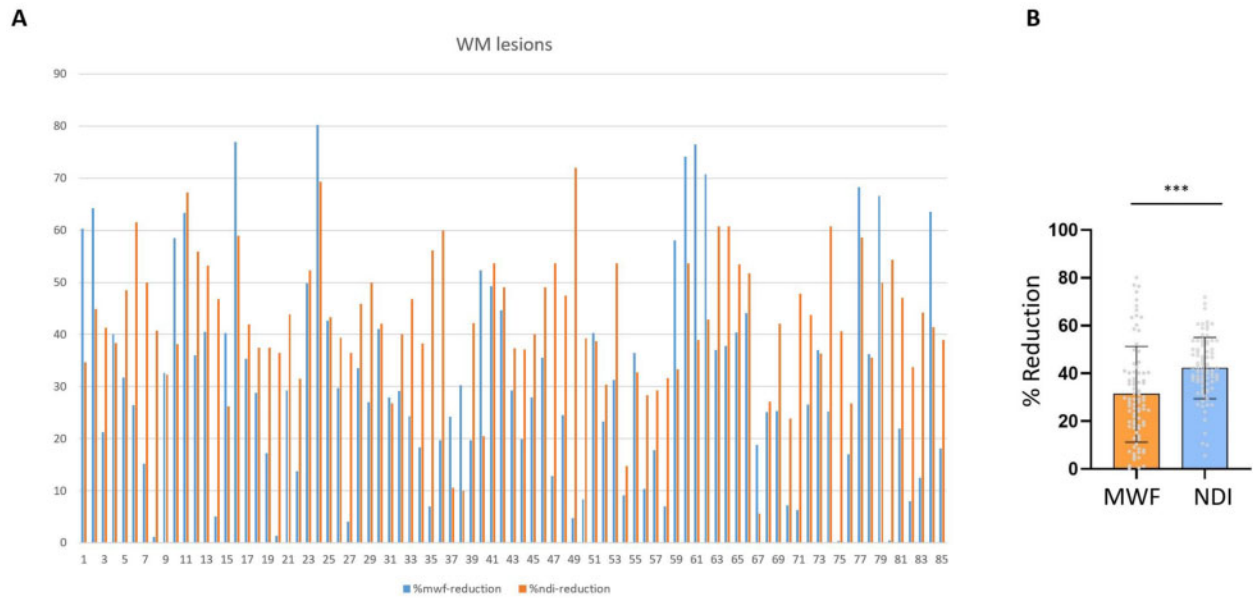


Figure 5 Alteration in MWF versus NDI in multiple sclerosis white matter lesions. (A) Percentage of MWF and NODDI-NDI decline for individual white matter (WM) lesions relative to mirror region of interest in contralateral hemisphere (individual multiple sclerosis white matter lesions are shown with numbers). (B) Bar graph shows that NODDI-NDI decreases more than MWF in multiple sclerosis lesions (** $P < 0.0001$).

demyelinating antibodies and myelin-reactive immune cells from ventricles than other brain areas.^{53,54}

We also characterized the profiles of axon and myelin damage in chronic active lesions: those are plaques characterized by activated microglia/macrophages at the lesion border, which exhibit a paramagnetic rim on susceptibility weighted images.^{55,56} Neuropathological studies showed that those lesions are characterized by extensive and ongoing damage to both myelin and axons⁵⁶; also, a recent imaging study revealed that their presence is associated with higher disability in patients.⁵⁵ Extending these works, we showed *in vivo* that chronic active lesions contain substantially lower amounts of myelin and axons than other multiple sclerosis lesions, hereby shedding light into the mechanisms driving increased disability in multiple sclerosis patients with this type of lesion compared to patients without.

Furthermore, when we compared the relative myelin and axonal content among white matter lesions, it appeared that—in a large majority of lesions—axonal damage outweighed myelin damage. Interestingly, this finding did not seem to be influenced by the anatomical location of white matter lesions, since we did not observe differences between periventricular, juxtacortical and deep white matter lesions. Higher axon than myelin damage in white matter lesions may be caused by differences in lesion age and remyelinating capacity.^{6,48,57} Alternatively or in addition, it may be due to a primary axonal pathology, as previously suggested.^{45,58,59} On the other hand, since we normalized the axon/myelin content by the corresponding NAWM in the contralateral hemisphere, the variability in NAWM damage may have in part influenced our assessment; similarly, our measurements may have been influenced by a different degree of sensitivity to myelin and axonal damage of MWF and NDI, respectively, although previous MRI-pathological studies suggest that it is similar.^{17,18,60}

In NAWM, we measured a widespread MWF and NDI reduction compared to the corresponding areas in healthy subjects, with a prevalent decrease in NDI. Remarkably, we did not find any difference in myelin or axonal content in NAWM between RRMS and PMS patients. Numerous previous imaging studies showed alterations in NAWM in multiple sclerosis patients.¹²

Reduced magnetization transfer ratio, increased T_2 and T_1 relaxation times, or altered mean diffusivity were reported in NAWM, suggesting various degrees of white matter microstructural alterations outside multiple sclerosis lesions.^{61–64} Adding to previous knowledge, we have now shown a broader decrease in axonal density than in myelin content in NAWM. Consistent with our results, neuropathological investigations of NAWM have shown that primary demyelination, in contrast to microglial activation and axonal transection, is not a frequent finding in NAWM.^{10,11,65}

With respect to the cortex, our vertex-wise analysis showed focal areas of myelin and axon damage throughout the NAGM, which were more extensive in PMS than in RRMS. Neuropathology studies also showed widespread neuronal loss and demyelination in NAGM, which might be associated with meningeal inflammatory infiltrates that are particularly evident in PMS.^{10,11} In accordance, MTI^{66,67} and DTI^{68,69} showed lower magnetization transfer ratio, lower fractional anisotropy, and higher mean diffusivity in NAGM of multiple sclerosis patients, with a more robust change in PMS compared to RRMS.

A pivotal finding of this study is the presence of axonal damage independent of demyelination in both focal white matter lesions and in NAWM. These findings are also in line with previous spectroscopy studies showing a very early diffuse reduction of a *N*-acetylaspartate in NAWM in RRMS patients⁷⁰ and an increase in lipid levels at the site of future multiple sclerosis lesions.⁷¹ Pathologically, this may be related to primary oligodendrocytopathy leading to axonal damage via disruption of oligodendrocyte-neuron cross-talk^{72–74} or to direct damage to the neuroaxonal unit.^{75–77}

It is still unclear whether RRMS and PMS are different entities or different presentations of the same entity. Our data show that distribution of axon and myelin pathology in both focal lesions and in NAWM is similar between RRMS and PMS, which is coherent with neuropathological studies suggesting that lesions in PMS and RRMS are qualitatively similar.^{2,78} Nonetheless, we also found remarkably widespread reductions in myelin and axonal content

in NAGM in PMS compared to RRMS patients, which may explain the different clinical phenotype.

Last, we found that imaging surrogate markers of myelin and axon pathology in white matter lesions—and not in normal-appearing tissues—are correlated with disability and serum neurofilaments. This is in line with previous reports by showing that magnetization transfer ratio—another surrogate measure of both myelin and axonal damage—is mostly related to disability when measured in lesions and not in the normal-appearing tissue⁷⁹ but apparently contradicts other works showing that NAWM/NAGM abnormalities are related to disability.^{80,81} The latter, however, were mostly univariate studies, which focused solely on the contribution of normal-appearing tissue abnormalities to disability, without taking lesion properties into account.

Interestingly, the associations between those imaging markers and disability/serum neurofilaments were evident and stronger in patients with clinical deficits only compared to patients with no disability. Those patients exhibited very heterogeneous damage in lesions but overall shorter disease duration than patients with EDSS > 1 (median disease duration 2.4 versus 7.7 years; $P < 0.01$). Hence, it may well be that those patients experience a higher functional reserve and more effective mechanisms compensating for structural damages, which is often the case at early disease stages.⁸²

Methodologically, we applied MWF and NDI, which provide surrogate—not direct—markers of myelin and axon characteristics. Despite their sensitivity and specificity already having been separately assessed in post-mortem studies,^{13,19} future work should focus on providing knowledge on their sensitivity/specificity in relationship to each other. Also, the study of MWF suffers from the limitation of non-isotropic voxel acquisitions, which may have decreased the sensitivity to myelin damage. On the other hand, NODDI suffers from the limitation of assuming a fixed diffusivity for all the voxels in the brain tissue, which may hamper its sensitivity and specificity. Because of this, we confirmed the results obtained with NODDI-NDI by using MCDMI-NDI, another model applicable to multi-shell diffusion data that estimates the diffusivity voxel-wise. Last, we did not acquire diffusion data with multiple echo times,⁸³ which would have helped to minimize the influence of myelin-water on NDI estimation: however, we statistically modelled the contribution of both NDI and MWF to the separation of lesion, normal-appearing and healthy tissue, hereby showing that NDI is providing statistically independent information from MWF to achieve an optimal separation of tissue types in white matter. Future work should further expand the current findings by attempting to achieve a better specificity of NDI maps, through targeted data acquisition schemes.

In conclusion, by applying advanced MRI measures we have further characterized the complex interplay between myelin and axon damage *in vivo* in multiple sclerosis patients. Our data extend existing knowledge from previous imaging studies and are compatible with concepts derived from neuropathology. Longitudinal studies are warranted to explore the temporal dynamics of pathological changes in brain microstructure in multiple sclerosis.

Acknowledgements

We thank all the patients and healthy subjects for taking part in this study and Marguerite Limberg for her work in enrolling patients into the study.

Funding

R.R. is supported by the MSIF-ECTRIMS McDonald fellowship, Multiple Sclerosis International Federation (MSIF-ECTRIMS.2019)

and the Swiss Government Excellence Scholarship (Nr.2019.0539). C.G. is funded by the Swiss National Science Foundation (SNSF) grant PP00P3_176984, the Stiftung zur Förderung der gastroenterologischen und allgemeinen klinischen Forschung, EUROSTAR E! 113682 HORIZON2020. F.L.R. is supported by the European Union's Horizon 2020 research and innovation program under the Marie Skłodowska-Curie project TRABIT (agreement # 765148). M.A. is supported by the Conrad N. Hilton foundation (grant # 17313). D.S.R., P.S., and M.A. are partially funded by the Intramural Research Program of the National Institute of Neurological Disorders and Stroke, National Institutes of Health, USA. M.W. is paid by the Swiss National Science Foundation (SNSF) grant PP00P3_176984 and he has also received research funding by Biogen for developing spinal cord MRI.

Competing interests

The authors report no competing interests.

Supplementary material

Supplementary material is available at *Brain* online.

References

1. Lassmann H. Pathogenic mechanisms associated with different clinical courses of multiple sclerosis. *Front Immunol.* 2018;9:3116.
2. Lucchinetti C, Brück W, Parisi J, Scheithauer B, Rodriguez M, Lassmann H. Heterogeneity of multiple sclerosis lesions: Implications for the pathogenesis of demyelination. *Ann Neurol.* 2000;47(6):707–717.
3. Barnett MH, Prineas JW. Relapsing and remitting multiple sclerosis: Pathology of the newly forming lesion. *Ann Neurol.* 2004; 55(4):458–468.
4. Metz I, Weigand SD, Popescu BF, et al. Pathologic heterogeneity persists in early active multiple sclerosis lesions. *Ann Neurol.* 2014;75(5):728–738.
5. Patani R, Balaratnam M, Vora A, Reynolds R. Remyelination can be extensive in multiple sclerosis despite a long disease course. *Neuropathol Appl Neurobiol.* 2007;33(3):277–287.
6. Patrikios P, Stadelmann C, Kutzelnigg A, et al. Remyelination is extensive in a subset of multiple sclerosis patients. *Brain.* 2006; 129(Pt 12):3165–3172.
7. Kuhlmann T, Ludwin S, Prat A, Antel J, Brück W, Lassmann H. An updated histological classification system for multiple sclerosis lesions. *Acta Neuropathol.* 2017;133(1):13–24.
8. Lieury A, Chanal M, Androdias G, et al. Tissue remodeling in periplaque regions of multiple sclerosis spinal cord lesions. *Glia.* 2014;62(10):1645–1658.
9. Mustafi SM, Harezlak J, Kodiweera C, et al. Detecting white matter alterations in multiple sclerosis using advanced diffusion magnetic resonance imaging. *Neural Regen Res.* 2019;14(1): 114–123.
10. Kutzelnigg A, Lucchinetti CF, Stadelmann C, et al. Cortical demyelination and diffuse white matter injury in multiple sclerosis. *Brain.* 2005;128(Pt 11):2705–2712.
11. Marik C, Felts PA, Bauer J, Lassmann H, Smith KJ. Lesion genesis in a subset of patients with multiple sclerosis: A role for innate immunity? *Brain.* 2007;130(Pt 11):2800–2815.
12. Enzinger C, Barkhof F, Ciccarelli O, et al. Nonconventional MRI and microstructural cerebral changes in multiple sclerosis. *Nat Rev Neurol.* 2015;11(12):676–686.
13. Laule C, Moore GRW. Myelin water imaging to detect demyelination and remyelination and its validation in pathology. *Brain Pathol.* 2018;28(5):750–764.

14. Cercignani M, Gandini Wheeler-Kingshott C. From micro- to macro-structures in multiple sclerosis: What is the added value of diffusion imaging. *NMR Biomed*. 2019;32(4):e3888.
15. Kozłowski P, Rosicka P, Liu J, Yung AC, Tetzlaff W. In vivo longitudinal Myelin Water Imaging in rat spinal cord following dorsal column transection injury. *Magn Reson Imaging*. 2014;32(3):250–258.
16. Moore GR, Leung E, MacKay AL, et al. A pathology-MRI study of the short-T2 component in formalin-fixed multiple sclerosis brain. *Neurology*. 2000;55(10):1506–1510.
17. Zhang H, Schneider T, Wheeler-Kingshott CA, Alexander DC. NODDI: Practical in vivo neurite orientation dispersion and density imaging of the human brain. *Neuroimage*. 2012;61(4):1000–1016.
18. Colgan N, Siow B, O'Callaghan JM, et al. Application of neurite orientation dispersion and density imaging (NODDI) to a tau pathology model of Alzheimer's disease. *Neuroimage*. 2016;125:739–744.
19. Grussu F, Schneider T, Tur C, et al. Neurite dispersion: A new marker of multiple sclerosis spinal cord pathology? *Ann Clin Transl Neurol*. 2017;4(9):663–679.
20. Bagnato F, Franco G, Thomas N, Smith S, Dortch R, Xu J. Multi-compartment spherical microscopic diffusion imaging using spherical mean techniques to probe axonal injury in multiple sclerosis. *Neurology*. 2018;P3:383.
21. Kaden E, Kelm ND, Carson RP, Does MD, Alexander DC. Multi-compartment microscopic diffusion imaging. *Neuroimage*. 2016;139:346–359.
22. Marques JP, Kober T, Krueger G, van der Zwaag W, Van de Moortele PF, Gruetter R. MP2RAGE, a self bias-field corrected sequence for improved segmentation and T1-mapping at high field. *Neuroimage*. 2010;49(2):1271–1281.
23. Sati P, George IC, Shea CD, Gaitan MI, Reich DS. FLAIR: A combined MR contrast technique for visualizing white matter lesions and parenchymal veins. *Radiology*. 2012;265(3):926–932.
24. Thompson AJ, Banwell BL, Barkhof F, et al. Diagnosis of multiple sclerosis: 2017 revisions of the McDonald criteria. *Lancet Neurol*. 2018;17(2):162–173.
25. Lublin FD, Reingold SC, Cohen JA, et al. Defining the clinical course of multiple sclerosis: The 2013 revisions. *Neurology*. 2014;83(3):278–286.
26. Kurtzke JF. Rating neurologic impairment in multiple sclerosis: An expanded disability status scale (EDSS). *Neurology*. 1983;33(11):1444–1452.
27. Nguyen TD, Deh K, Monohan E, et al. Feasibility and reproducibility of whole brain myelin water mapping in 4 minutes using fast acquisition with spiral trajectory and adiabatic T2prep (FAST-T2) at 3T. *Magn Reson Med*. 2016;76(2):456–465.
28. De Graaf RA, Nicolay K. Adiabatic rf pulses: Applications to in vivo NMR. *Concepts Magn Reson*. 1997;9(4):247–268.
29. Kumar D, Nguyen TD, Gauthier SA, Raj A. Bayesian algorithm using spatial priors for multiexponential T(2) relaxometry from multiecho spin echo MRI. *Magn Reson Med*. 2012;68(5):1536–1543.
30. Veraart J, Novikov DS, Christiaens D, Ades-Aron B, Sijbers J, Fieremans E. Denoising of diffusion MRI using random matrix theory. *Neuroimage*. 2016;142:394–406.
31. Andersson JLR, Sotiropoulos SN. An integrated approach to correction for off-resonance effects and subject movement in diffusion MR imaging. *Neuroimage*. 2016;125:1063–1078.
32. Absinta M, Sati P, Fechner A, Schindler MK, Nair G, Reich DS. Identification of chronic active multiple sclerosis lesions on 3T MRI. *AJNR Am J Neuroradiol*. 2018;39(7):1233–1238.
33. Liu T, Xu W, Spincemaille P, Avestimehr AS, Wang Y. Accuracy of the morphology enabled dipole inversion (MEDI) algorithm for quantitative susceptibility mapping in MRI. *IEEE Trans Med Imaging*. 2012;31(3):816–824.
34. La Rosa F, Abdulkadir A, Fartaria MJ, et al. Multiple sclerosis cortical and white matter lesion segmentation at 3T MRI: A deep learning method based on FLAIR and MP2RAGE. *Neuroimage Clin*. 2020;27:102335.
35. Geurts JJ, Rosendaal SD, Calabrese M, et al. Consensus recommendations for multiple sclerosis cortical lesion scoring using double inversion recovery MRI. *Neurology*. 2011;76(5):418–424.
36. Fischl B. FreeSurfer. *Neuroimage*. 2012;62(2):774–781.
37. Jenkinson M, Beckmann CF, Behrens TE, Woolrich MW, Smith SM. Fsl. *Neuroimage*. 2012;62(2):782–790.
38. Vrenken H, Geurts JJ, Knol DL, et al. Normal-appearing white matter changes vary with distance to lesions in multiple sclerosis. *AJNR Am J Neuroradiol*. 2006;27(9):2005–2011.
39. Disanto G, Barro C, Benkert P, et al. Serum neurofilament light: A biomarker of neuronal damage in multiple sclerosis. *Ann Neurol*. 2017;81(6):857–870.
40. Firth D. Bias reduction of maximum likelihood estimates. *Biometrika*. 1993;80:27–38.
41. Reich DS, Lucchinetti CF, Calabresi PA. Multiple sclerosis. *N Engl J Med*. 2018;378(2):169–180.
42. Androdias G, Reynolds R, Chanal M, Ritleng C, Confavreux C, Nataf S. Meningeal T cells associate with diffuse axonal loss in multiple sclerosis spinal cords. *Ann Neurol*. 2010;68(4):465–476.
43. Ingram G, Loveless S, Howell OW, et al. Complement activation in multiple sclerosis plaques: An immunohistochemical analysis. *Acta Neuropathol Commun*. 2014;2:53.
44. Frischer JM, Bramow S, Dal-Bianco A, et al. The relation between inflammation and neurodegeneration in multiple sclerosis brains. *Brain*. 2009;132(Pt 5):1175–1189.
45. Stys PK, Zamponi GW, van Minnen J, Geurts JJ. Will the real multiple sclerosis please stand up? *Nat Rev Neurosci*. 2012;13(7):507–514.
46. Bruck W. Inflammatory demyelination is not central to the pathogenesis of multiple sclerosis. *J Neurol*. 2005;252(Suppl 5):v10–v15.
47. Goldschmidt T, Antel J, König FB, Bruck W, Kuhlmann T. Remyelination capacity of the multiple sclerosis brain decreases with disease chronicity. *Neurology*. 2009;72(22):1914–1921.
48. Lucchinetti C, Bruck W, Parisi J, Scheithauer B, Rodriguez M, Lassmann H. A quantitative analysis of oligodendrocytes in multiple sclerosis lesions. A study of 113 cases. *Brain*. 1999;122(Pt 12):2279–2295.
49. Bodini B, Veronese M, Garcia-Lorenzo D, et al. Dynamic imaging of individual remyelination profiles in multiple sclerosis. *Ann Neurol*. 2016;79(5):726–738.
50. Boyd A, Zhang H, Williams A. Insufficient OPC migration into demyelinated lesions is a cause of poor remyelination in multiple sclerosis and mouse models. *Acta Neuropathol*. 2013;125(6):841–859.
51. Lürbke A, Hagemeyer K, Cui Q-L, et al. Limited TCF7L2 expression in multiple sclerosis lesions. *PLoS One*. 2013;8(8):e72822.
52. Schultz V, van der Meer F, Wrzos C, et al. Acutely damaged axons are remyelinated in multiple sclerosis and experimental models of demyelination. *Glia*. 2017;65(8):1350–1360.
53. Magliozzi R, Howell O, Vora A, et al. Meningeal B-cell follicles in secondary progressive multiple sclerosis associate with early onset of disease and severe cortical pathology. *Brain*. 2007;130(Pt 4):1089–1104.
54. Wings KM, Gilden DH, Bennett JL, Yu X, Ritchie AM, Owens GP. Analysis of multiple sclerosis cerebrospinal fluid reveals a continuum of clonally related antibody-secreting cells that are

- predominantly plasma blasts. *J Neuroimmunol.* 2007;192(1-2):226–234.
55. Absinta M, Sati P, Masuzzo F, et al. Association of chronic active multiple sclerosis lesions with disability in vivo. *JAMA Neurol.* 2019;76:1474.
 56. Dal-Bianco A, Grabner G, Kronnerwetter C, et al. Slow expansion of multiple sclerosis iron rim lesions: Pathology and 7 T magnetic resonance imaging. *Acta Neuropathol.* 2017;133(1):25–42.
 57. Solanky M, Maeda Y, Ming X, et al. Proliferating oligodendrocytes are present in both active and chronic inactive multiple sclerosis plaques. *J Neurosci Res.* 2001;65(4):308–317.
 58. Stadelmann C. Multiple sclerosis as a neurodegenerative disease: Pathology, mechanisms and therapeutic implications. *Curr Opin Neurol.* 2011;24(3):224–229.
 59. Trapp BD, Nave KA. Multiple sclerosis: An immune or neurodegenerative disorder? *Annu Rev Neurosci.* 2008;31:247–269.
 60. Laule C, Leung E, Lis DK, et al. Myelin water imaging in multiple sclerosis: Quantitative correlations with histopathology. *Mult Scler.* 2006;12(6):747–753.
 61. Bonnier G, Roche A, Romascano D, et al. Advanced MRI unravels the nature of tissue alterations in early multiple sclerosis. *Ann Clin Transl Neurol.* 2014;1(6):423–432.
 62. Filippi M. MRI measures of neurodegeneration in multiple sclerosis: Implications for disability, disease monitoring, and treatment. *J Neurol.* 2015;262(1):1–6.
 63. Inglese M, Bester M. Diffusion imaging in multiple sclerosis: Research and clinical implications. *NMR Biomed.* 2010;23(7):865–872.
 64. Schmierer K, Scaravilli F, Altmann DR, Barker GJ, Miller DH. Magnetization transfer ratio and myelin in postmortem multiple sclerosis brain. *Ann Neurol.* 2004;56(3):407–415.
 65. Bjartmar C, Kinkel RP, Kidd G, Rudick RA, Trapp BD. Axonal loss in normal-appearing white matter in a patient with acute multiple sclerosis. *Neurology.* 2001;57(7):1248–1252.
 66. Ge Y, Grossman RI, Udupa JK, Babb JS, Mannon LJ, McGowan juxtacortical. Magnetization transfer ratio histogram analysis of normal-appearing gray matter and normal-appearing white matter in multiple sclerosis. *J Comput Assist Tomogr.* 2002;26(1):62–68.
 67. Samson RS, Cardoso MJ, Muhlert N, et al. Investigation of outer cortical magnetisation transfer ratio abnormalities in multiple sclerosis clinical subgroups. *Mult Scler.* 2014;20(10):1322–1330.
 68. Ceccarelli A, Rocca MA, Falini A, et al. Normal-appearing white and grey matter damage in multiple sclerosis. A volumetric and diffusion tensor MRI study at 3.0 Tesla. *J Neurol.* 2007;254(4):513–518.
 69. Rovaris M, Bozzali M, Iannucci G, et al. Assessment of normal-appearing white and gray matter in patients with primary progressive multiple sclerosis: A diffusion-tensor magnetic resonance imaging study. *Arch Neurol.* 2002;59(9):1406–1412.
 70. Narayana PA, Doyle TJ, Lai D, Wolinsky JS. Serial proton magnetic resonance spectroscopic imaging, contrast-enhanced magnetic resonance imaging, and quantitative lesion volumetry in multiple sclerosis. *Ann Neurol.* 1998;43(1):56–71.
 71. Filippi M, Rocca MA, Martino G, Horsfield MA, Comi G. Magnetization transfer changes in the normal appearing white matter precede the appearance of enhancing lesions in patients with multiple sclerosis. *Ann Neurol.* 1998;43(6):809–814.
 72. Cui QL, Khan D, Rone M, et al. Sublethal oligodendrocyte injury: A reversible condition in multiple sclerosis? *Ann Neurol.* 2017;81(6):811–824.
 73. Howell OW, Rundle JL, Garg A, Komada M, Brophy PJ, Reynolds R. Activated microglia mediate axoglial disruption that contributes to axonal injury in multiple sclerosis. *J Neuropathol Exp Neurol.* 2010;69(10):1017–1033.
 74. Ozawa K, Suchanek G, Breitschopf H, et al. Patterns of oligodendroglia pathology in multiple sclerosis. *Brain.* 1994;117(Pt 6):1311–1322.
 75. Bitsch A, Schuchardt J, Bunkowski S, Kuhlmann T, Bruck W. Acute axonal injury in multiple sclerosis. Correlation with demyelination and inflammation. *Brain.* 2000;123(Pt 6):1174–1183.
 76. Srivastava R, Aslam M, Kalluri SR, et al. Potassium channel KIR4.1 as an immune target in multiple sclerosis. *N Engl J Med.* 2012;367(2):115–123.
 77. Yan W, Nguyen T, Yuki N, et al. Antibodies to neurofascin exacerbate adoptive transfer experimental autoimmune neuritis. *J Neuroimmunol.* 2014;277(1-2):13–17.
 78. Antel J, Antel S, Caramanos Z, Arnold DL, Kuhlmann T. Primary progressive multiple sclerosis: Part of the multiple sclerosis disease spectrum or separate disease entity? *Acta Neuropathol.* 2012;123(5):627–638.
 79. Amann M, Papadopoulou A, Andelova M, et al. Magnetization transfer ratio in lesions rather than normal-appearing brain relates to disability in patients with multiple sclerosis. *J Neurol.* 2015;262(8):1909–1917.
 80. Manfredonia F, Ciccarelli O, Khaleeli Z, et al. Normal-appearing brain t1 relaxation time predicts disability in early primary progressive multiple sclerosis. *Arch Neurol.* 2007;64(3):411–415.
 81. Ramio-Torrenta L, Sastre-Garriga J, Ingle GT, et al. Abnormalities in normal appearing tissues in early primary progressive multiple sclerosis and their relation to disability: A tissue specific magnetisation transfer study. *J Neurol Neurosurg Psychiatry.* 2006;77(1):40–45.
 82. Lopez-Gongora M, Escartin A, Martinez-Horta S, et al. Neurophysiological evidence of compensatory brain mechanisms in early-stage multiple sclerosis. *PLoS One.* 2015;10(8):e0136786.
 83. Gong T, Tong Q, He H, Sun Y, Zhong J, Zhang H. MTE-NODDI: Multi-TE NODDI for disentangling non-T2-weighted signal fractions from compartment-specific T2 relaxation times. *Neuroimage.* 2020;217:116906.